Soft Matter

The influence of roughness on stem cell differentiation using 3D printed Polylactic acid scaffolds

Journal:	*Soft Matter*
Manuscript ID	SM-ART-09-2018-001797.R1
Article Type:	Paper
Date Submitted by the Author:	13-Nov-2018
Complete List of Authors:	Feng, Kuan-Che; Stony Brook University, Material Science and Chemical Engineering Pinkas-Sarafova, Adriana; Stony Brook University, Material Science and Chemical Engineering Ricotta, Vincent; Stony Brook University, Material Science and Chemical Engineering Cuiffo, Michael; Stony Brook University Guo, Yichen; Stony Brook University, Materials Science and Engineering Zhang, Linxi; Stony Brook University Chang, Chung-Chueh; Advanced Energy Center, ThINC Facility Ceter Halada, Gary; Stony Brook University, Materials Science & Engineering Simon, Marcia; Stony Brook School of Dental Medicine, Oral Biology and Pathology Rafailovich, Miriam; Stony Brook University, Materials science and Engineering

Soft Matter

ARTICLE

The influence of roughness on stem cell differentiation using 3D printed Polylactic acid scaffolds

Received 00th January 20xx,
Accepted 00th January 20xx

DOI: 10.1039/x0xx00000x

www.rsc.org/

Kuan-Che Feng[a], Adriana Pinkas-Sarafova[a], Vincent Ricotta[a], Michael Cuiffo[a], Linxi Zhang[a], Yichen Guo[a], Chung-Chueh Chang[b], Gary P. Halada[a], Marcia Simon[c] and Miriam Rafailovich[a]

With the increase in popularity of 3D printing, an important question arises as to the equivalence between devices manufactured by standard methods vs. those presenting with identical bulk specifications, but manufactured via fused deposition modeling (FDM) printing. Using thermal imaging in conjunction with electron and atomic force microscopy, we demonstrate that large thermal gradients, whose distribution is difficult to predict, are associated with FDM printing and result in incomplete fusion and sharkskin of the printing filament. Even though these features are micro or submicron scale, and hence may not interfere with the intended function of the device, they can have a profound influence if the device comes in contact with living tissue. Dental pulp stem cells were cultured on substrates of identical dimensions, which were either printed or molded from the same PLA stock material. The cultures exhibited significant differences in plating efficiency, migration trajectory, and morphology at early times stemming from attempts by the cells to minimize cytoplasm deformation as they attempt to adhere on the printed surfaces. Even though biomineralization without dexamethasone induction was observed in all cultures at later times, different gene expression patterns were observed on the two surfaces. (Osteogenic markers were upregulated on molded substrates, while odontogenic markers were upregulated on the FDM printed surfaces) Our results clearly indicate that the method of manufacturing is an important consideration in comparing devices, which come in contact with living tissues.

Introduction

With recent advances in the field of additive technology, it has become evident that biomedical devices are a particularly appropriate application for additive manufacturing since the method could print devices directly from Computer Tomography (CT) [1] or ultrasound scans [2] and hence tailor the device specifically to the individual [3]. In order to obtain FDA approval for their use, in most cases, the industry is arguing for the application of the FDA 510(k) criterion, where minimal additional research is required to obtain clearance since the specifications of the final devices manufactured by both methods are so similar.

Polylactic acid (PLA) has become the most sought-after polymer for Fused Deposition Modeling (FDM) 3D printing[4]. It is, a natural polymer, first synthesized by polycondensation of lactic acid in 1845, and has long been a popular material in bioengineering [5]. PLA is rigid, yet shock absorbent, and crystalline[4], but still ductile with a relatively low glass-transition temperature (T_g) around 60°C, and melting point (T_m) of 160°C [6, 7]. Furthermore, PLA is biodegradable and has been declared by the FDA to be biocompatible it is also a favorite material for use in osteo-repair elements, such as bone implants, bone screws, and prosthetics for craniofacial malformations[6]. In these applications, PLA is used as a mechanical support and scaffold promoting osseointegration of the host bone, and being resorbed as the physiological repair process takes over. Currently these devices are manufactured mostly by traditional extrusion or molding [8, 9], where a great deal is already known regarding the interaction of the devices with cells, tissue and fluids[10-16]. When specifications for implants are posted, their criteria usually refer to macroscopic properties, such as mechanical response, goodness of fit, and anti-bacterial character. The

[a] Department of Materials Science and Chemical Engineering, Stony Brook University, Stony Brook, NY 11794
[b] ThINC Facility, Advanced Energy Center, Stony Brook University, Stony Brook, NY 11794
[c] Department of Oral Biology and Pathology, Stony Brook University, Stony Brook, NY 11794

biocompatibility requirement usually refers to inflammatory response or thrombogenicity. Rarely do the specifications also refer to the intrinsic micro and nanoscale structure of the surfaces or the nanoparticle inclusions. Hence, even if the bulk specifications are identical, different manufacturing methods can induce differences in the nanostructures of the finished material. For example, Kanev et al have shown that PLA fibers extruded under different flow rates develop a periodic surface roughness, also known as "shark skin", which arises from slip/stick behavior at the output of the extruder [17]. The amplitude and the periodicity of the sharkskin ranged from nano to micro-scaled features depending on the extrusion speed and the interaction between the polymer and the surface of the extrusion nozzle [18, 19].

If the amplitude of the roughness is small compared to the other dimensions of the device, it generally does not affect the macroscopic flow properties or mechanical performance, and hence is not a consideration in determining eligibility for the 510(k) clearance.

In the case of devices that come in contact with blood, or other tissues, where cell migration or attachment can occur, the roughness of the surface can make a profound difference in the interaction with the tissue, since numerous recent studies, such as those by Souness et al which added microstructure purposely,[20] have reported that cells can sense these structures and modify their response [10-15].

This raises an important concern regarding the interaction of cells and implantable devices, where the integration of the device and the body depends not only on the chemical nature of the material or its macroscopic thermo-mechanical response, but it may also depend on the process with which the device was manufactured.

To address this question, we have performed a study where cell scaffolds were either molded, using standard extrusion processes, or 3D printed using a MakerBot Replicator™ 2 Desktop 3D FDM printer. We chose to focus on PLA for this study since it is a well-characterized biomedical material and it is also one of the most popular materials in the 3D printing industry [9, 21]. Due to its high modulus, PLA is frequently used in dentistry and orthopedics [22].

For this study we therefore chose to probe the interaction between dental pulp derived cells which can differentiate along odontogenic, osteogenic, neurogenic or adipogenic pathways [23], and soft matter scaffolds which were either molded using standard polymer processing procedures versus scaffolds of identical dimensions, but produced via 3D FDM printing.

Materials and Methods

Substrate Preparation

In order to eliminate surface chemistry as a variable, all substrates were prepared from identical PLA source materials, namely, MakerBot 1.75 mm spool PLA filament. Molded substrates were prepared by manually pelletizing the filament and placing the pellets into 12mm diameter, 2mm thick stainless steel molds, sandwiched between Kapton sheets, and placed in a Carver Hot Press at 180°C and 5psi for approximately 5 minutes. The substrates where then air-cooled, removed from the molds, and stored in tissue culture plates for sterilization.

The substrates used in the cell plating studies were printed using a MakerBot Replicator™ 2 Desktop 3D Printer at an extrusion temperature of 230°C and approximate speed of 60mm/s. The samples were printed using MakerBot filaments, with the same dimensions as the molded ones, namely 2mm thick and 12 mm in diameter, printed at 100% infill.

Sample Sterilization

Due to the low glass-transition temperature around 60°C of PLA, autoclaving, which reaches temperatures in excess of 120°C with high humidity is not an appropriate sterilization technique. The samples were therefore sterilized by exposure to ethylene oxide (EtO), using the standard procedures[24] and described in greater detail in various application notes[25]. The procedure was performed at the Stony Brook University Hospital Central Sterilize Facility where the samples were heated at 55°C in 48% humidity at 570mBar.

Cell isolation and culture

Dental pulp cells (DPCs) strain AV3-GFP were isolated from the third molar teeth (IRB #20076778)[26-28], and were transduced to express enhanced green fluorescent protein (eGFP), which enabled us to continuously track cell growth without fixing or staining.

Furthermore, this enabled us to use epifluorescence microscopy since the samples were opaque and could only be imaged in reflection mode. For all experiments, 6th pass of AV3-GFP cells was used and cultures were grown in α–MEM media (Life Technologies) supplemented with 10% fetal bovine serum, 200μM L-ascorbic acid 2-phosphate and 100 units/ml penicillin, and 100μg/ml streptomycin.

Cell Culture and proliferation

All substrates were placed in 6-well plates (Falcon). AV3-GFP-DPCs were plated on all substrates (9,000 cells/cm^2) in 4 ml medium (α-MEM, 10% fetal bovine serum, 200μM L-ascorbic acid, 100 units/ml penicillin, 100μg/ml streptomycin). After 24 hours, all scaffolds were moved to new 6-well plates with fresh media to avoid cell growth on the tissue culture plate and affect the experiment. The medium was changed with α-MEM containing 10% fetal bovine serum, 200μM L-ascorbic acid, 100 units/ml penicillin, 100μg/ml streptomycin and 10mM β-glycerol phosphate, following by media change every other day. For the study of cell proliferation, the cell number was determined on day 1 and 5 using a hemocytometer (Hausser Scientific)

Fluorescent Microscopy

On the first day and every other day, DPCs were observed and imaged by fluorescent microscopy (Olympus CK40). The three-dimensional images of cell cultures, and mobility video images were obtained using a Leica confocal microscope where NucBlue Live Cell Stain (Molecular Probes) was used to stain the cell nuclei. Samples were imaged at day 28 and day 42.

RNA isolation and RT-PCR

RNA was isolated from cells cultured on the substrates made by either 3D printing or molding after 28 days and 42 days, using RNeasy® Plus Universal Mini Kit (QIAGEN) following the manufacturer's protocol. RNA concentrations were determined by absorbance at 260nm; 2 μg of total RNA was reverse transcribed with SuperScriptTM II RT and random primers (Invitrogen) following the protocol by the manufacturer. Real-time PCR samples were performed in triplicate in Opticon 2 at the DNA sequencing facility of Stony Brook University. The expression levels of bone alkaline phosphatase (ALP) and osteocalcin (OCN), osteonectin (ON), Collagen type I alpha 1 (COL1A1), dentin sialoprotein (DSPP) and bone sialoprotein (BSP) were determined using the gene specific primers listed in table 1. Results were analyzed by Opticon software and normalized by 18S RNA. Gene expression upregulation was calculated on the base day one of plating.

Table 1: Primers used for determination of gene expression

Primer	Direction	Primer Sequence 5' to 3'	Product Size (bp)
18S	F	GTAACCCGTTGAACCCCATT	151
	R	CCATCCAATCGGTAGTAGCG	
ALP	F	GTACTGGCGAGACCAAGCGCAA	282
	R	ACCCCACACAGGTAGGCGGT	
OCN	F	ATGAGAGCCCTCACACTCCTCG	255
	R	GTCAGCCAACTCGTCACAGTCC	
COLI a1	F	AGGCTGGTGTGATGGGATTC	129
	R	GAGCTCCAGCCTCTCCATCT	
DSPP	F	AATGCTGGAGCCACAAAC	248
	R	GCTTCCTTAGTCCCATTTC	
BSP	F	ACGATTTCCAGTTCAGGGCA	212
	R	ACCCTGTATACCCTGTGCCA	

	F	GGCTCAAGAACGTCCTGGT	
ON			374
	R	CTGCTTGATGCCGAAGCAG	

Scanning Electron Microscopy (SEM)

The morphology of the printed and molded polymer samples was determined using scanning electron microscopy (SEM, Jeol JSM7600F). Samples for SEM were washed with deionized water to remove the salt from the media and put in the desiccator under vacuum to dry for one day. All the samples were coated with 10 nm thickness of gold on the surfaces to increase electrical conductivity. Surface topographies of 3D printed and molded substrates and cell morphologies were characterized using the SEM at 2.5keV accelerating voltage using secondary electron detectors with 45-degree tilt angle.[6] In addition, 42-day culture samples were characterized using the scanning electron microscopy at 20keV accelerating voltage using backscattering electron detectors, and elemental contents of deposits on the surface were measured by Energy Dispersive X-ray spectroscopy (EDX) with SEM.

Results and Discussion

PLA scaffold analysis

It is a well-established phenomenon that, when cells interact with materials they sense surface chemistry, mechanical features and topography [10-15]. Therefore, in our study, we produced a set of scaffold discs via thermal molding and 3D printing at 100% fill using a MakerBot Replicator™ 2 Desktop 3D Printer, using the same commercially MakerBot 1.75 mm PLA spool material. We chose a simple flat design such that the only unknown parameter would be the method of processing.

The samples were then sterilized with Ethylene oxide (EtO), using a standard hospital protocol, and the ATR-FTIR spectra were performed. The molded and printed filaments have shown no significant different from those of virgin PLA before or after sterilization, as previously reported by Kister and Peniston[29, 30]. Contact angle goniometry was also performed on the samples and the results are shown in figure 1A. From the figure we see a slight increase in hydrophobicity following sterilization for both types of samples. The increase was also reported previously by Valente, et al [31]. The increase is the same for both cases, indicating that any chemical modifications that occurred were similar in both surfaces [32]. From that we conclude that the differences in contact angles between the molded and printed surfaces are, as will be shown later, due to differences in surface roughness.

In figure 1B a thermal image of the filament being extruded from the nozzle is shown together with a photographic image in the insert. From the figure we see that the temperature of the filament directly at the exit of the nozzle is greater than 150°C, or out of the range of our camera. Within a few millimeters the filament has cooled to 102°C, which is lower than the melting temperature of PLA. The full thermal profile of a single pass of the nozzle is shown below; where we find that the freshly deposited filament cools rapidly to 80°C within seconds after passage of the nozzle. The filament in the lower layer is also shown, where we see that it has cooled to 50°C, which is less than T_g of PLA preventing proper adhesion between consecutive fiber, layers. This can also be seen in figure 1C where we show SEM images of a sample fractured in liquid nitrogen and imaged in cross section, we can clearly see that the filament structure is still distinct, with porous regions between the filament layers, despite being printed with the 100% fill option. The internal structure indicates that despite the high temperature of the nozzle (230°C), the filaments are cooling rapidly after deposition and are unable to fuse completely. Due to the poor thermal conductivity of polymers, simulations of the surface temperatures of the filaments have shown that they can be significantly cooler than the actual nozzle temperature [33].

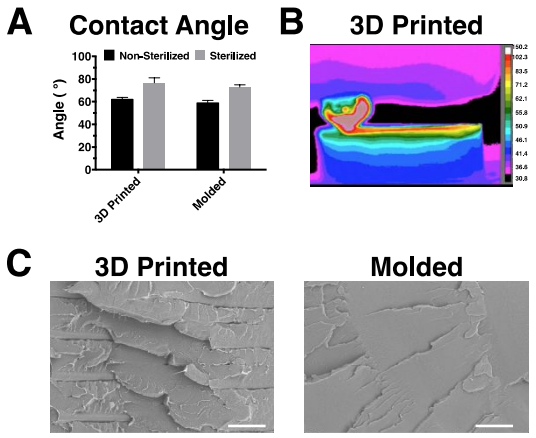

Figure 1. Scaffold analysis. (A) Water contact angle measured before and after ETO exposure to achieve sterility for both 3D printed and molded substrates. No significant difference is observed in water contact angle between the two surfaces either before exposure to after exposure to ETO, which slightly increases the degree of hydrophobicity for both surfaces. (B) Thermal image obtained with the FLIR camera while printing a sample with the MakerBot ReplicatorTM. The image shows the PLA filament cool rapidly after extrusion. (C) SEM image of cross section on 3D printed scaffolds and molded scaffolds.

In figure 2 we show SEM of the sample surfaces. From the figure we see that the surfaces of the molded samples (2B) are quite smooth, while those of the printed (2A) samples exhibit multi scale roughness. At the low magnification (1K) images we see that the filament structure on the surface remains distinct, contributing roughness, and with a well-defined period, corresponding to the fiber diameter. At higher (10K) magnification when focused on the structure of the individual fibers, a periodic roughness appears with a period of several micrometers. The height of these features is best measured using scanning force microscopy, as shown in figure 2C, where an RMS roughness of the molded surfaces is less than 7 nm while that of the printed surface is larger than 360 nm.

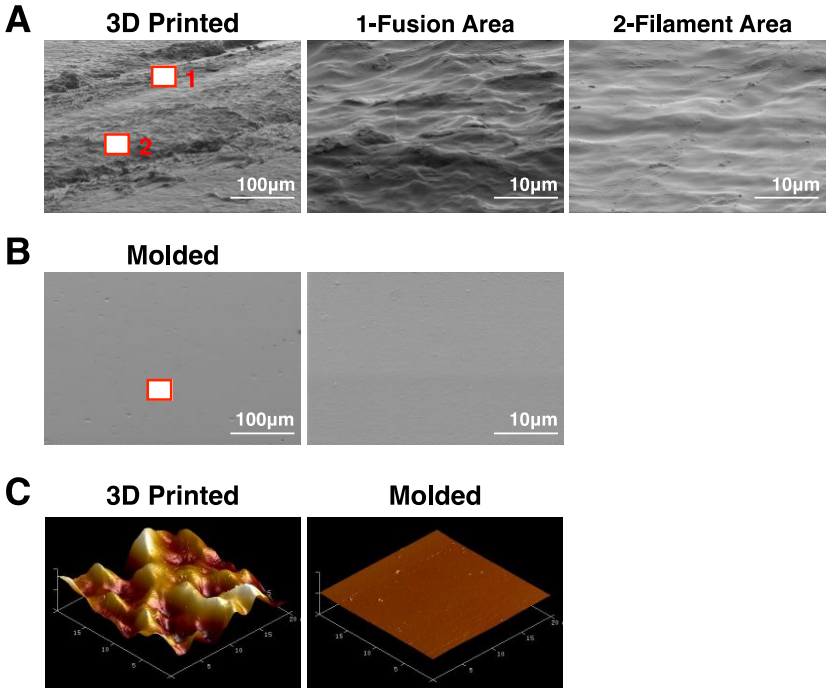

Figure 2. Topographic characterization of PLA scaffolds. (A,B) SEM images of regions from the surface of the 3D printed samples showing the roughness profiles obtained in the area where two filaments are fused and on the filament, and molded scaffold surface. (C) AFM analysis of 3D printed and molded surface, RMS roughness of the 3D printed surface is 367.5 nm and molded surfaces is 6.75 nm.

We postulate that the periodic roughness observed on the printed surface is the results of sharkskin that is formed during the extrusion process. The sharkskin occurs at the point of exit of the filament from the nozzle where the temperature is highest. The sample cools rapidly after the filament is deposited preserving the sharkskin patterns on the sample surface, which is superimposed on

the pattern of the incompletely fused fibers. The conditions leading to the formation of sharkskin on PLA fibers was discussed by Miller et al, [18] where they showed that the effect originates from slip/stick of the polymer extruded from the nozzle, and the periodicity is a function of the extrusion rate and the nozzle diameter. The shear rate, Υ, can be estimated from the equation

$$\dot{\gamma}_a = \frac{4Q}{\pi R^3}$$

$$\gamma_w = \frac{\gamma_a}{4}(3 + \frac{1}{n})$$

where Q=0.0075cm^3/s is the flow rate at the extrusion speed used of 60mm/sec, 2R =0.4mm is the diameter for the nozzle, n=0.65, is the power law index for PLA [34], and therefore the estimated shear rate is, Υ_w= 1360 S^{-1}. This value is similar to the one obtained by Kanev, et al, [17] where they observed sharkskin in PLA in the micrometer range.

In order to determine which other parameters of the FDM printing process contribute to sharkskin, we varied the printing temperature and the printing speed and used atomic force microscopy to measure the surface topography and RMS roughness of the printed discs. The results are plotted in figure 3A and tabulated in table 2, where we find that the most critical parameter is the printing speed. Only minimal variation was found when only the temperature was varied within the range 210°C<T<230°C. All temperatures in the range studied were above T_m~160°C, and hence the interface with the nozzle involved molten polymer, which could adsorb strongly to the metal interface. This behavior is again consistent with that previously report[17]. In table 2 we plot the values of Υ_w which corresponding to the printing speeds used to produce the samples shown in figure 3. From the figure we can see that regardless of temperature, the surface roughness increases abruptly at Υ_w~1360, which is in good agreement with Υ_w>1000, or the value where they observed the onset of sharkskin roughness[17].

Table 2: Shear rate related to printing speed.

Printing speed	Υ_w
25mm/s	567 S^{-1}
30mm/s	680 S^{-1}
50mm/s	1135 S^{-1}
60mm/s	1360 S^{-1}
100mm/s	2269 S^{-1}

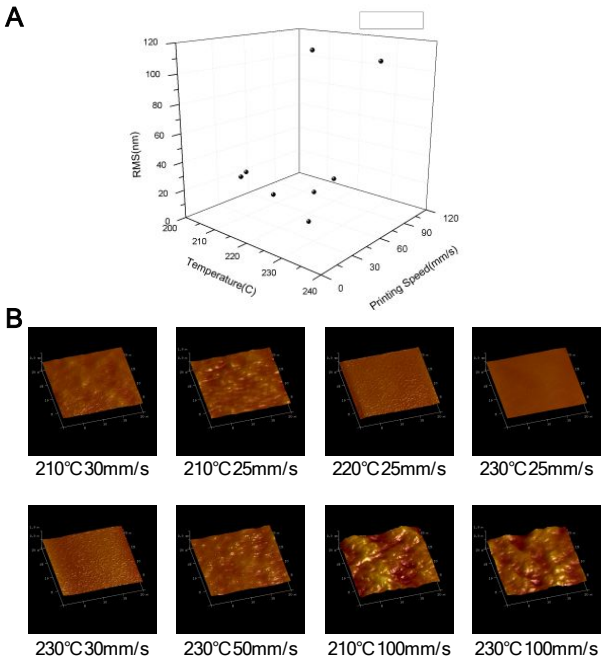

Figure 3 Printing parameters affect surface roughness. (A) Different printing speed and temperature related to scaffold surface RMS roughness. (B) AFM images show surface roughness with different printing parameters.

Interactions of DPC with 3D printed and molded scaffolds:

Cell attachment, proliferation, and migration (dynamics at early stages)

There is a large body of literature that documents the profound influence of surface roughness with different order, length scale, and amplitude on stem cell fate (9-14). In this case, the FDM printing process produces surfaces where all these scales can co-exist without any specific order and with random amplitude and intensity.

In order to determine the impact of the FDM 3D printed surface topography on primary cell cultures, we chose to plate GFP

expressing dental pulp derived cells on both printed and molded scaffolds, made from the identical PLA polymer fiber stock, and evaluate their attachment, migration, proliferation, and differentiation. Averaging over the data from seven independent experiments, we plot the plating efficiencies for the two types of substrates in figure 3D, where we find that the plating efficiency is significantly lower ($p<0.01$) in each case on the printed surfaces. The substrate influence on cell morphology, 24 hours after plating, can also be seen in figure 3A, where the cells plated on the molded substrates are significantly more elongated. This quantification by comparing their axial ratios (r), on the two surfaces shows dramatic differences in the adhesion profiles, where the cells plated on the 3D printed surfaces have much smaller axial ratios, r= 2.9±0.7, with an average length of 45.7±7.2µm as compared to cells plated on the molded surfaces which have, r= 7.0±3.1, and the average length 98.9±34.1µm (figure 4A). SEM images of the cells after 5 days in culture are shown in figure 4C where we can see that on the molded samples, the cells are highly extended and making good contact with the surface along their entire length. In contrast the cells on the 3D printed scaffolds (figure 4D) are barely touching the substrate. From the figure we can see that the cells are clearly minimizing contact with the rough surface features. In fact, the cells appear to form bridges across area with very small features. From the images one can see that in order for cells to adhere to surfaces with nanoscale roughness, large deformations of the cell membrane, with appropriate distortions of the cytoplasm and cytoskeleton must occur in order for the cell body to conform to the surface topography. Hence the cells assume the bridge structure, which minimizes the deformation.

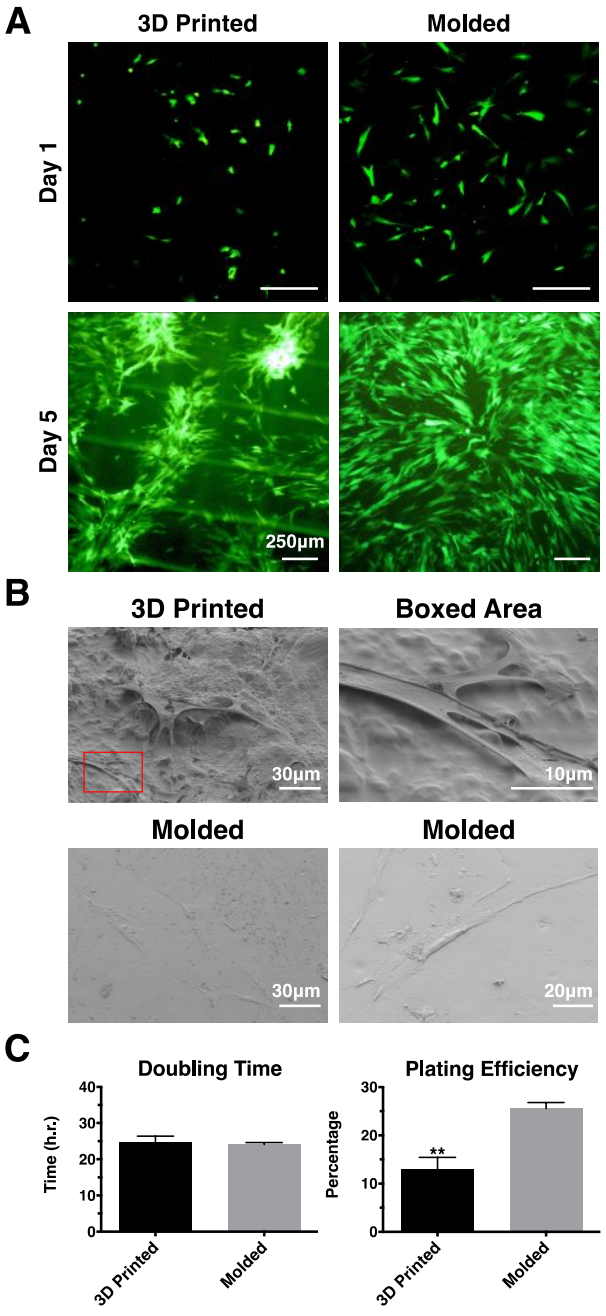

Figure 4. Cell attachment at early stage. (A) Day 1 fluorescent pictures show there are more cells sitting on the molded samples than 3D printed samples. The cells distribute more evenly on the molded samples than 3D printed samples. Day 5 the cells on the 3D sample are clustered along topographical regions while those on the molded sample are distributed more evenly. (Scale bars are 250µm) (B) Day 3 SEM images of cells show the cell seat differently on the 3D printed and molded surface. (C) The plating efficiency is significantly different between the cells on 3D printed and molded surface. However, the doubling times on both surfaces are similar.

The cell proliferation rates were also measured and found to be similar for both substrates, somewhat longer than 24 hours, the literature value obtained on TCP. Differences between the substrates, as shown in figure 4D, though, were not significant;

hence the differences in morphology did not appear to affect proliferation.

In figure 4B we show the fluorescent microscope image of the cells 5 days after incubation. Comparing the two surfaces, we can immediately see that the distribution of cells is very different between the two surfaces. On the molded substrates the cells are uniformly distributed across the sample surface, while on the 3D printed substrates cell aggregates are formed where the cells appear to be oriented along the rough features associated with the underlying fibers. In this case cells appear to be clustered in high-density groupings along the incompletely fused fibers protruding from the surface. Hence the cells in certain areas, such as the crevices, are confluent while those in the higher areas are not. On the molded surface the cells have uniform degree of confluence across the entire sample surface. Hence we investigated in further details some of the cell functions which are known to be impacted by confluence [35]. For example, cell dynamics is an important factor in the formation of tissue at early stages. Video images of the growing culture were obtained for 10 hours between day 3 and 4 and a typical trajectory of the nucleus for one cell migrating on either the printed and molded samples is shown in Figures 5A. The path length and end-to-end distance of the trajectories traveled by 15 cells on each of the surfaces were measured and the average values are plotted in figures 5B and 5C. From the figure we can see that the total path length traveled in the same time interval is not significantly different between the molded and printed samples, and hence the migration speed is similar on the two types of surfaces. On the other hand from figure 5C we find that the end to end distance is nearly twice as long ($p<0.01$) on the molded than on the printed surface, consistent with the formation of cell clusters which prefer to be confined in the recessed areas of the substrate. Furthermore, it is also consistent with the inability of the cells to find an appropriate location for attaching to the surface. Hence the cells migrate over longer distances as they search for the surface patterns, which allow them to adhere with minimal deformation.

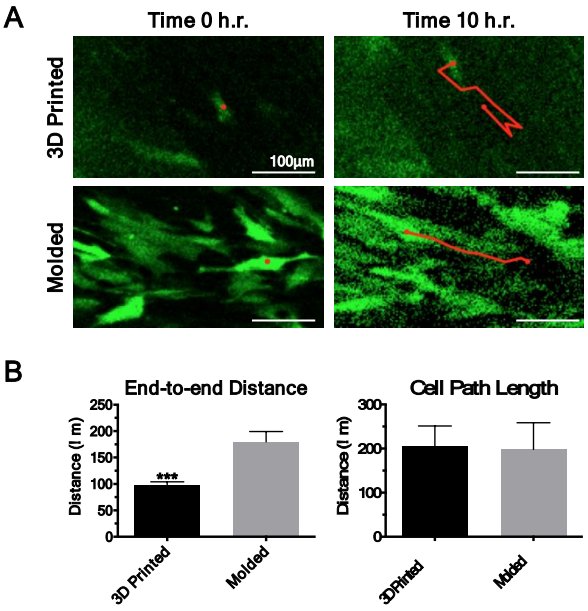

Figure 5. Cell migration. (A) The continuous confocal pictures show the pathway of the cells on the 3D printed samples and molded samples in 10 hours. (Scale bars are 100µm) (B) The cell path length is almost the same but the end-to-end distance is significantly different (n=10).

Influence of substrate on DPSC differentiation

In order to observe only the influence of the processing method on differentiation DPSC cultures were incubated for 28 and 42 days without addition of dexamethasone, the standard cytokine used to initiate differentiation. Confocal images of the cells after incubation for 28 days on molded and printed substrates are shown in figure 6. Figures 6A are three-dimensional view of the entire tissue where multiple layers of cells are observed on each substrate. It is interesting to note that the tissue is conformal to the general outline of the filaments (shown as an arc, of radius 100 microns, delineated on the image) on the interface adjacent to the substrate. In figures 6B we show a top view of the first layer cells immediately at the air interface and the layer of cells adjacent to the substrate, as marked in figure 6A. The morphology of the cells in the top layer is the same regardless of substrate. Namely the cells are well extended and the layer is confluent. On the other hand, the morphology of the layer immediately adjacent to the substrate differs markedly between the two substrates. On the molded substrate, the top and bottom layers are similar with nearly identical aspect ratio. On the other hand, on the printed substrates, the aspect ratios are significantly different ($p<0.05$). The cells adjacent to the substrate are not well extended and follow the

contours of the rough features shown in the SEM images. Their aspect ratio (r<3.0) is more similar to that of the cells imaged on day one of incubation, consistent with our observation that the cells have a confined trajectory. As the cells proliferate, the available space becomes even more constricted, and the cells in the bottom layer remained pinned along the surface features. Their orientation though does not seem to propagate further into the tissue, such that the cells in the upper layers have similar conformation to the control and the molded samples.

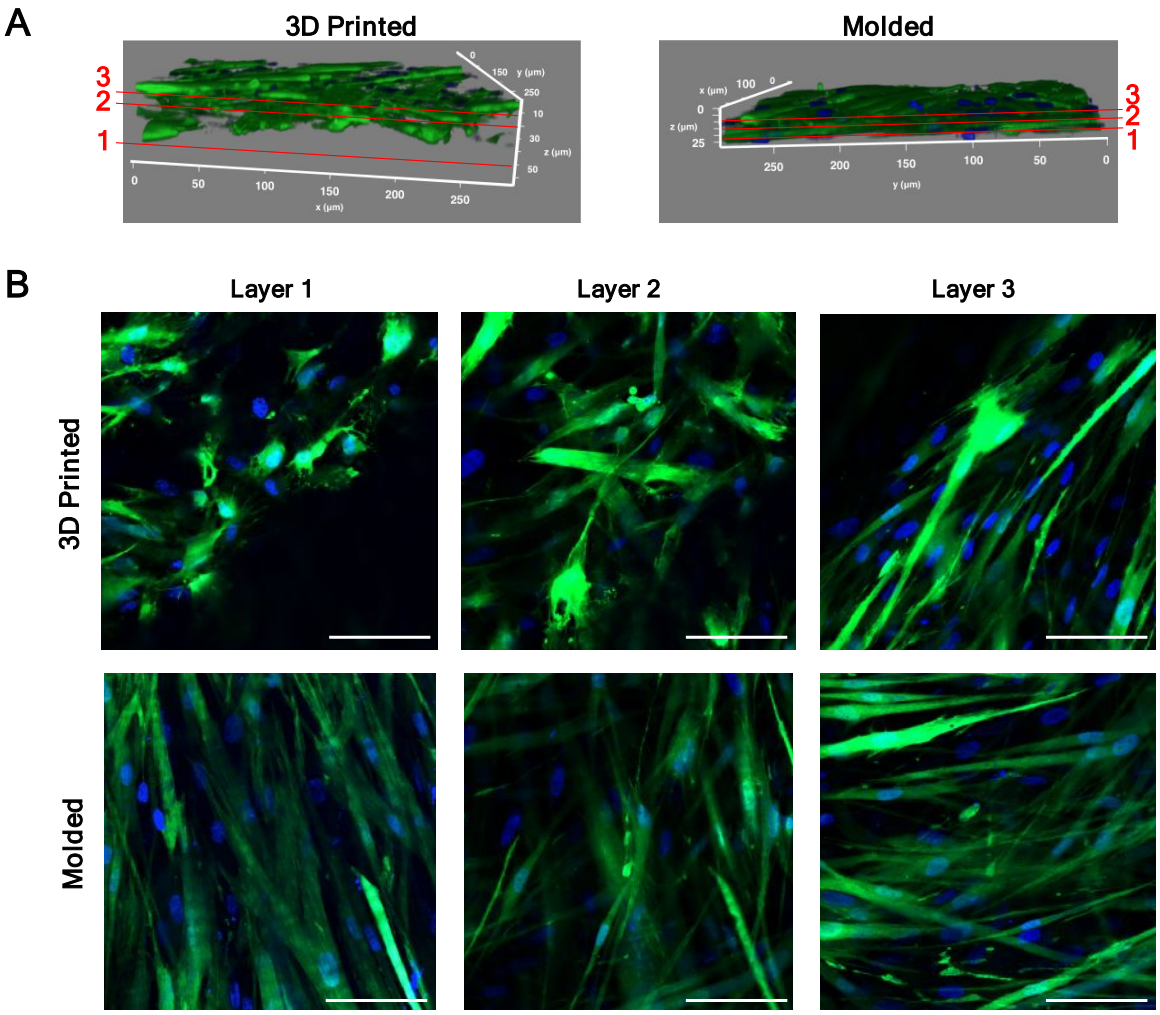

Figure 6. Day 28 confocal image. (A) The day 28 3D projection images of the cells on 3D printed and molded surface from confocal. (B) The day 28 confocal images, showing the top layer cells on both samples are stretching and align similarly. The cells at the bottom layer on 3D printed samples are stretching and align differently due to the surface difference. (Scale bars are 75μm)

The scaffolds from the 42-day incubation were imaged with SEM/EDX in order to determine whether biomineral deposition had occurred. Low magnification backscattered images are shown in figure 7A, where the calcium deposits, having higher atomic number than the polymer matrix, appear brighter than the background. As seen on the figure on the printed scaffolds large biomineral deposits can be observed deposited fairly uniformly across the scaffold. Excess deposition is observed

along the boundaries between fibers where the roughness is largest. Higher magnification images are shown in the corner, where the granular morphology typical of hydroxyl apatite is clearly seen covering large areas of the surface. This is further confirmed by the EDX spectra obtained over a large surface area, which are identical to those obtained from a small area focused on a particle. The spectra are typical of hydroxyl apatite, where both calcium and phosphate peaks are clearly seen. Similar analysis was also performed on the molded scaffolds, where similar deposits are observed, but at a lower density. EDX spectra confirm that these deposits are hydroxyl apatite as well. Hence from these images we can confirm that the DPSC had biomineralized on both types of scaffolds in the absence of dexamethasone.

In order to determine their gene expression profile RT-PCR was performed at days 28 and 42. The results are shown in figure 7B where the data is plotted relative to day 1 and normalized by the housekeeping gene, 18S. From the figure we can see that at day 28, ALP, an early marker for differentiation is up regulated on both types of scaffolds, as is osteocalcin, a gene associated with osteogenic differentiation. No significant difference in the relative magnitudes for the expression of these genes between the two scaffolds is observed. On the other hand, a significant difference in the magnitude of DSPP, a gene associated with odontogenic, rather than osteogenic lineage, can already be detected, where upregulation occurs mostly on the printed scaffold. This is further confirmed from the RT-PCR results obtained at day 42. From the figure we can see that ALP, an early stage marker, is down regulated on both substrates, as expected. Comparing the OCN and DSPP genes, we see that OCN clearly remains upregulated only on the molded scaffold, while DSPP upregulation dominates only the printed scaffold, indicating that the biomineral deposition on the two scaffolds could be attributed to two different cell lineages; osteogenic in the case of the smoother molded scaffold, and odontogenic in the case of the multi-scaled rough printed scaffold.

These results clearly indicate that the surface can determine the differentiation lineage of the sample. RT-PCR measures the genetic expression of the entire tissue, yet, the confocal image above only one layer, which represents at most approximately 20% of the total cell count that is in contact with the substrate, reflects its morphology. The robust signal observed indicates that the ondontogenic gene expression may not be limited to the first layer, and may propagate throughout the tissue. The exact mechanism has yet to be determined.

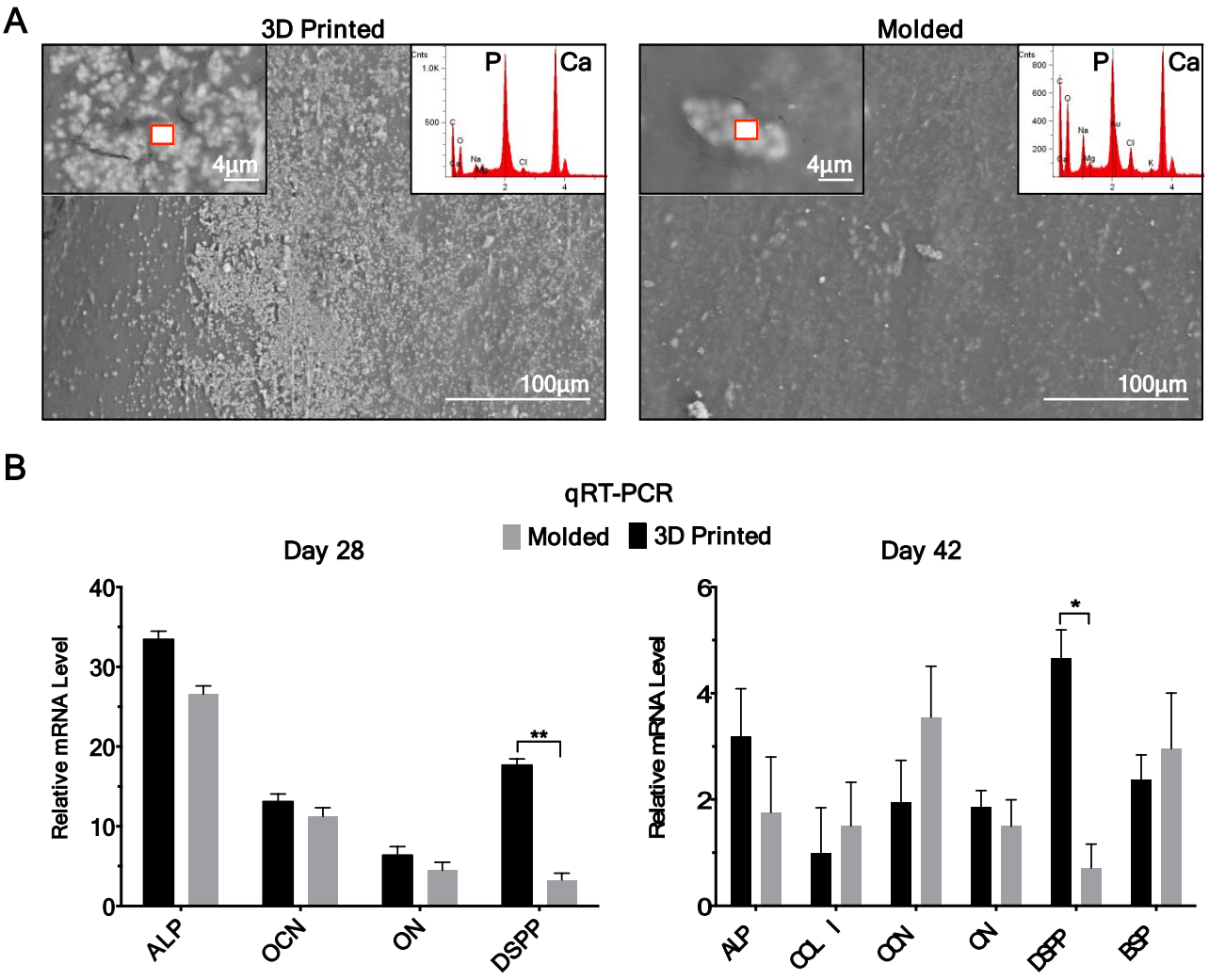

Figure 7 Biomineralization and differentiation. (A) SEM images of the dried scaffolds after 42 days in culture. Inset: Associated EDX of the area corresponding to the region outlined in the red boxes. (B) RT-PCR result between Molded and 3D printed samples at day 28 and day 42.

Conclusion

We have shown that substantive differences can exist at the micro and submicron scale between structures produced via standard molding protocols and three-dimensional FDM printing with identical bulk specification. Thermal imaging of the FDM printing process clearly shows rapid cooling and poor thermal propagation between layers that leads to incomplete fusion of filaments and surface sharkskin formation. Primary cell cultures plated on molded and FDM printed surfaces exhibit differences in cell morphology, plating efficiency, and migration trajectories within the first few days in culture. These differences persist within the layer adjacent to the substrate, and even though they disappear within the higher layers, they determine the choice of lineage. After 42 days only osteogenic differentiation markers were observed on the molded substrates, while a distinct odontogenic marker was upregulated on the FDM printed surfaces. These results clearly indicate that in addition to the bulk specification, the method of manufacturing needs to be considered in comparing devices which come in contact with living tissues.

Conflicts of interest

There are no conflicts to declare.

Acknowledgement

We gratefully acknowledge the support of the National Science Foundation (NSF grant INSPIRE#1344267) and the ThINC facility at the Stony Brook Advanced Energy Center for imaging and characterization.

Reference

1. L. Ibáñez, 3D print your medical scan, http://makezine.com/projects/make-42/3d-print-your-medical-scan/, (accessed Aug 24, 2017).
2. S. B. Kesner and R. D. Howe, *Mechatronics, IEEE/ASME Transactions On*, 2011, **16**, 866-870.
3. C. L. Ventola, *P T*, 2014, **39**, 704-711.
4. C. A. Murphy and M. N. Collins, *Polym. Compos.*, 2018, **39**, 1311-1320.
5. H. Benninga, *A history of lactic acid making: a chapter in the history of biotechnology*, Springer Science & Business Media, 1990.
6. Y. Guo, K. Yang, X. Zuo, Y. Xue, C. Marmorat, Y. Liu, C.-C. Chang and M. H. Rafailovich, *Polymer*, 2016, **83**, 246-259.
7. Y. Guo, S. He, K. Yang, Y. Xue, X. Zuo, Y. Yu, Y. Liu, C.-C. Chang and M. H. Rafailovich, *ACS applied materials & interfaces*, 2016, **8**, 17565-17573.
8. S. Yang, K.-F. Leong, Z. Du and C.-K. Chua, *Tissue engineering*, 2002, **8**, 1-11.
9. Y. Guo, C.-C. Chang, M. A. Cuiffo, Y. Xue, X. Zuo, S. Pack, L. Zhang, S. He, E. Weil and M. H. Rafailovich, *Polymer Degradation and Stability*, 2017, **137**, 205-215.
10. J. Y. Lim and H. J. Donahue, *Tissue engineering*, 2007, **13**, 1879-1891.
11. C. M. Conde, F. F. Demarco, L. Casagrande, J. C. Alcazar, J. E. Nör and S. B. C. Tarquinio, *Brazilian dental journal*, 2015, **26**, 93-98.
12. G. B. Schneider, R. Zaharias, D. Seabold, J. Keller and C. Stanford, *Journal of Biomedical Materials Research Part A*, 2004, **69**, 462-468.
13. K. Kolind, D. Kraft, T. Bøggild, M. Duch, J. Lovmand, F. S. Pedersen, D. A. Bindslev, C. Bünger, M. Foss and F. Besenbacher, *Acta Biomater.*, 2014, **10**, 641-650.
14. D. Kim, J. Kim, H. Hyun, K. Kim and S. Roh, *Arch. Oral Biol.*, 2014, **59**, 765-774.
15. H. Nakamura, L. Saruwatari, H. Aita, K. Takeuchi and T. Ogawa, *Journal of dental research*, 2005, **84**, 515-520.
16. Y. Yu, Q. Zhang, C.-C. Chang, Y. Liu, Z. Yang, Y. Guo, Y. Wang, D. K. Galanakis, K. Levon and M. Rafailovich, *Analyst*, 2016, **141**, 5607-5617.
17. D. Kanev, E. Takacs and J. Vlachopoulos, *Int. Polym. Proc.*, 2007, **22**, 395-401.
18. E. Miller and J. P. Rothstein, *Rheologica Acta*, 2004, **44**, 160-173.
19. H. Hu, J. Liu, T. Sun, J. Zhao, X. Wang, C. Li, X. Dong and D. Wang, *RSC Advances*, 2016, **6**, 81703-81711.
20. A. Souness, F. Zamboni, G. M. Walker and M. N. Collins, *Journal of Biomedical Materials Research Part B: Applied Biomaterials*, 2018, **106**, 533-545.
21. E. Canessa, C. Fonda, M. Zennaro and N. DEADLINE, *Low-cost 3D printing for science, education and sustainable development*, 2013.
22. M. Molitch-Hou, Dentures get 3D printed boost with DENTCA's FDA approval, http://3dprintingindustry.com/news/dentures-get-3d-printed-boost-with-dentcas-fda-approval-55274/, (accessed Aug 10, 2015).
23. S. Gronthos, J. Brahim, W. Li, L. Fisher, N. Cherman, A. Boyde, P. DenBesten, P. G. Robey and S. Shi, *Journal of dental research*, 2002, **81**, 531-535.
24. *USA Pat.*, 2,189,947, 1940.
25. C. R. Phillips and S. Kaye, *American journal of hygiene*, 1949, **50**, 280-288.
26. S. Batouli, M. Miura, J. Brahim, T. Tsutsui, L. Fisher, S. Gronthos, P. G. Robey and S. Shi, *Journal of Dental Research*, 2003, **82**, 976-981.
27. C. Chang, A. Bherwani, M. Simon, M. Rafailovich and V. Jurukovski, *Ann J Materials Sci Eng*, 2014, **1**, 7.
28. L. Zhang, Y. Yu, C. Joubert, G. Bruder, Y. Liu, C.-C. Chang, M. Simon, S. G. Walker and M. Rafailovich, *Polymers*, 2016, **8**, 193.
29. G. Kister, G. Cassanas and M. Vert, *Polymer*, 1998, **39**, 267-273.
30. S. J. Peniston and S. J. Choi, *Journal of Biomedical Materials Research Part B: Applied Biomaterials*, 2007, **80**, 67-77.
31. T. Valente, D. Silva, P. Gomes, M. Fernandes, J. Santos and V. Sencadas, *ACS applied materials & interfaces*, 2016, **8**, 3241-3249.
32. M. A. Cuiffo, J. Snyder, A. M. Elliott, N. Romero, S. Kannan and G. P. Halada, *Applied Sciences*, 2017, **7**, 579.
33. S. C. Jake Lindberg, Marvin Huang, *JUCIER*, 2016, **5**, 61-66.
34. K. Hamad, M. Kaseem and F. Deri, *Asia-Pacific Journal of Chemical Engineering*, 2012, **7**, S310-S316.
35. A. Banfi, A. Muraglia, B. Dozin, M. Mastrogiacomo, R. Cancedda and R. Quarto, *Exp. Hematol.*, 2000, **28**, 707-715.